A proposed crystal structure of lifitegrast sesquihydrate Form A, $(C_{29}H_{24}Cl_2N_2O_7S)_2(H_2O)_3$

James A. Kaduk,[1,2,a] Megan M. Rost,[3] Anja Dosen,[3] and Thomas N. Blanton[3]
[1]*Illinois Institute of Technology, 3101 S. Dearborn St., Chicago, IL 60616, USA*
[2]*North Central College, 131 S. Loomis St., Naperville, IL 60540, USA*
[3]*ICDD, 12 Campus Blvd., Newtown Square, PA 19073-3273, USA*

(Received 18 June 2024; accepted 10 September 2024)

A proposed crystal structure of lifitegrast Form A has been derived using synchrotron X-ray powder diffraction data and optimized using density functional theory techniques. Lifitegrast sesquihydrate Form A crystallizes in space group $P2_1$ (#4) with $a = 18.2526(4)$, $b = 5.15219(6)$, $c = 30.1962(6)$ Å, $\beta = 90.8670(19)$, $V = 2839.35(7)$ Å^3, and $Z = 4$ at 295 K. The crystal structure consists of discrete lifitegrast molecules linked by hydrogen bonds among carboxylic acid groups, carbonyl groups, and water molecules into a three-dimensional framework. The water molecules occur in clusters. Each water molecule acts as a donor in two O–H···O hydrogen bonds, and as an acceptor. One water molecule acts as an acceptor in a water–water O–H···O hydrogen bond, and all three water molecules are acceptors in C–H···O hydrogen bonds. Each carboxylic acid group acts as a donor in a strong discrete O–H···O hydrogen bond; one to a water molecule and the other to a carbonyl group. The amino groups both form N–H···O hydrogen bonds to carbonyl groups. The powder pattern has been submitted to ICDD® for inclusion in the Powder Diffraction File™ (PDF®).

[doi:10.1017/S0885715624000459]

Key words: lifitegrast, Xiidra, crystal structure, Rietveld refinement, density functional theory

I. INTRODUCTION

Lifitegrast (marketed under the trade name Xiidra) is used for treatment of keratoconjunctivitis sicca (dry eye syndrome). The systematic name (CAS Registry Number 1025967-78-5) is (2S)-2-[[2-(1-benzofuran-6-carbonyl)-5,7-dichloro-3,4-dihydro-1H-isoquinoline-6-carbonyl]amino]-3-(3-methylsulfonylphenyl)propanoic acid. A two-dimensional molecular diagram of lifitegrast is shown in Figure 1.

Novel crystalline Forms A, B, C, D, and E of lifitegrast are claimed in US Patent 8,367,701 B2 (Burnier et al., 2013; SARcode Bioscience Inc.). A comparison of the powder pattern of this study to that of Form A reported by Burnier et al. confirms that our material is Form A (Figure 2). Crystalline Form A is specified as comprised of at least 98.5% of the *S*-enantiomer. Thermogravimetric analysis of Form A indicated a mass loss of 2.5 wt.%, showing that this form is a hydrate.

This work was carried out as part of a project (Kaduk et al., 2014) to determine the crystal structures of large-volume commercial pharmaceuticals and include high-quality powder diffraction data for them in the Powder Diffraction File (Kabekkodu et al., 2024).

II. EXPERIMENTAL

Lifitegrast was a commercial reagent, purchased from TargetMol (Batch #153342), and was used as-received. The white powder was packed into a 1.5-mm diameter Kapton capillary and rotated during the measurement at ~50 Hz. The powder pattern was measured at 295 K at beamline 11-BM (Antao et al., 2008; Lee et al., 2008; Wang et al., 2008) of the Advanced Photon Source at Argonne National Laboratory using a wavelength of 0.459744(2) Å from 0.5

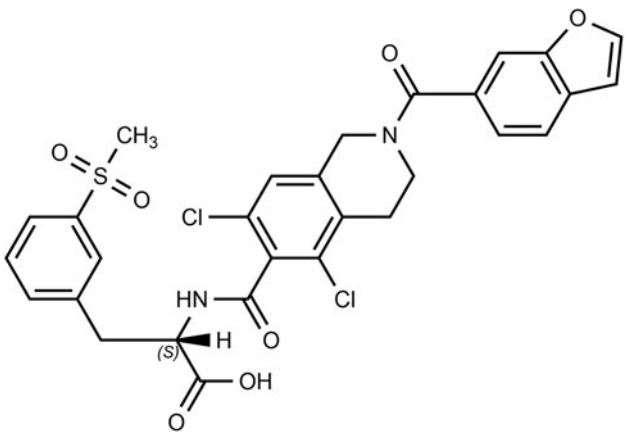

Figure 1. The two-dimensional structure of lifitegrast.

[a]Author to whom correspondence should be addressed. Electronic mail: kaduk@polycrystallography.com

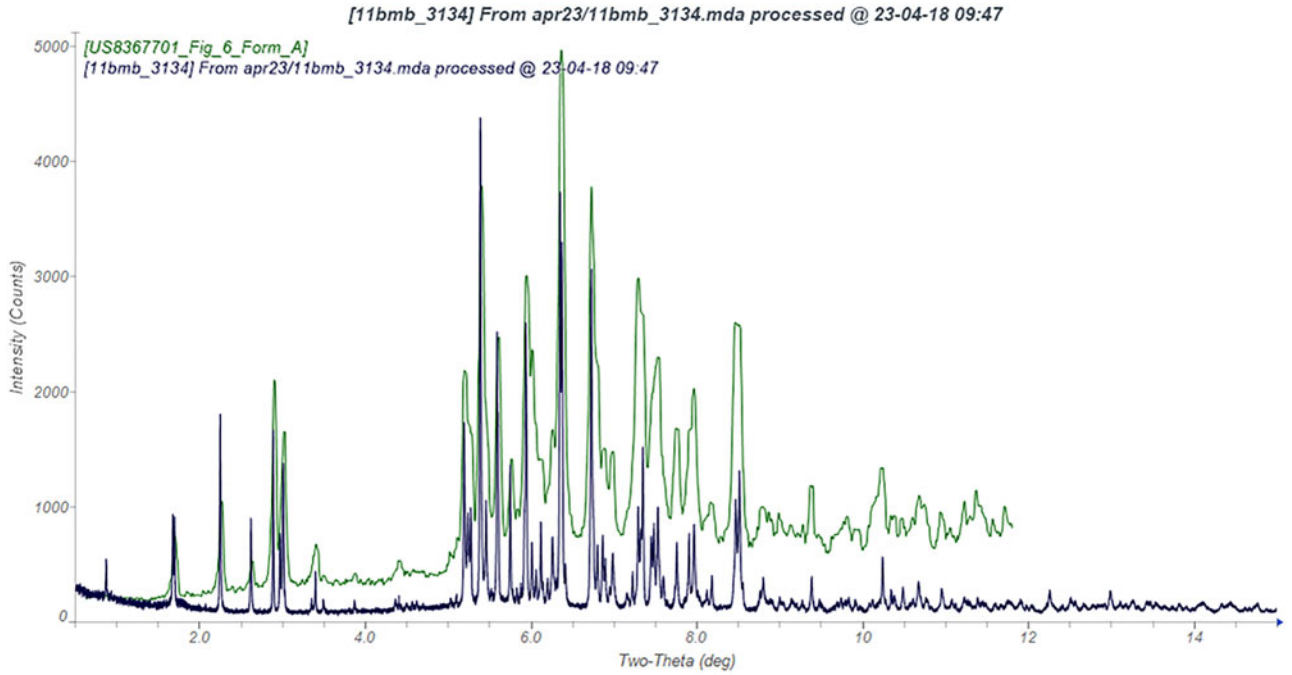

Figure 2. Comparison of the synchrotron pattern of lifitegrast (black) to that of Form A reported by Burnier et al. (2013; green). The literature pattern (measured using CuKα radiation) was digitized using UN-SCAN-IT (Silk Scientific, 2013) and converted to the synchrotron wavelength of 0.459744(2) Å using JADE Pro (MDI, 2024). Image generated using JADE Pro (MDI, 2024).

to 40° 2θ with a step size of 0.001° and a counting time of 0.1 s step^{-1}. The high-resolution powder diffraction data were collected using 12 silicon crystal analyzers that allow for high angular resolution, high precision, and accurate peak positions. A mixture of silicon (NIST SRM 640c) and alumina (NIST SRM 676a) standards (ratio Al_2O_3:Si = 2:1 by weight) was used to calibrate the instrument and refine the monochromatic wavelength used in the experiment.

The pattern was indexed with DICVOL14 (Louër and Boultif, 2014) using the Predict interface (Blanton et al., 2019; 20 peaks) on a primitive monoclinic unit cell with a = 18.2546, b = 5.0335, c = 30.2026 Å, β = 90.923°, and V = 2774.80 Å^3. The cell volume corresponds to approximately 4 lifitegrast molecules per cell. The space group suggested by EXPO2014 (Altomare et al., 2013) was $P2_1$, which was confirmed by successful solution and refinement of the structure. A reduced cell search in the Cambridge Structural Database (Groom et al., 2016) yielded 9 hits, but no lifitegrast derivatives.

The lifitegrast molecule was downloaded from PubChem (Kim et al., 2023) as Conformer3D_Compound_CID_11965427.sdf. It was converted to a *.mol2 file using Mercury (Macrae et al., 2020). The crystal structure was solved using Monte Carlo simulated annealing techniques as implemented in EXPO2014 (Altomare et al., 2013), using two lifitegrast molecules and two O atoms (water molecules) as fragments, with a <010> preferred orientation parameter (the anisotropy of the unit cell suggested that needle morphology was likely) and a bump penalty.

The structure was refined, and a moderate-sized void was noted. The void was large enough for a third water molecule, which would be stabilized by forming a number of hydrogen bonds. This model with an additional water molecule in the void region was optimized using the Forcite module of Materials Studio (Dassault Systèmes, 2023) and then with VASP (Kresse and Furthmüller, 1996) through the MedeA graphical interface (Materials Design, 2024). The structure was then re-refined, the hydrogen positions were recalculated using Materials Studio, and the structure was then re-optimized using VASP. The final crystal structure refinement used the result of the second VASP optimization for the initial positions.

Rietveld refinement was carried out with GSAS-II (Toby and Von Dreele, 2013). Only the 0.7–18.0° portion of the pattern was included in the refinements (d_{min} = 1.469 Å), as this was the region that contained Bragg peaks. All non-H bond distances and angles were subjected to restraints, based on a Mercury/Mogul Geometry Check (Bruno et al., 2004; Sykes et al., 2011). The Mogul average and standard deviation for each quantity were used as the restraint parameters. The benzene rings and the fused ring systems were restrained to be planar. The restraints contributed 7.1% to the overall χ^2. The hydrogen atoms were included in calculated positions, which were recalculated during the refinement using Materials Studio (Dassault Systèmes, 2023). The U_{iso} of the heavy atoms were grouped by chemical similarity. The U_{iso} for the H atoms were fixed at 1.3× the U_{iso} of the heavy atoms to which they are attached. The peak profiles were described using the generalized microstrain model (Stephens, 1999). The background was modeled using a 6-term shifted Chebyshev polynomial, with a peak at 5.81° to model the scattering from the Kapton capillary and an amorphous component.

The final refinement of 296 variables using 17 328 observations and 230 restraints yielded the residuals R_{wp} = 0.1579 and GOF = 2.06. The largest peak (1.23 Å from C101) and hole (1.56 Å from C83) in the difference Fourier map were 0.33(10) and −0.38(10) eÅ^{-3}, respectively. The final Rietveld plot is shown in Figure 3. The largest features in the normalized error plot are in the intensities of some

https://doi.org/10.1017/S0885715624000459 Published online by Cambridge University Press

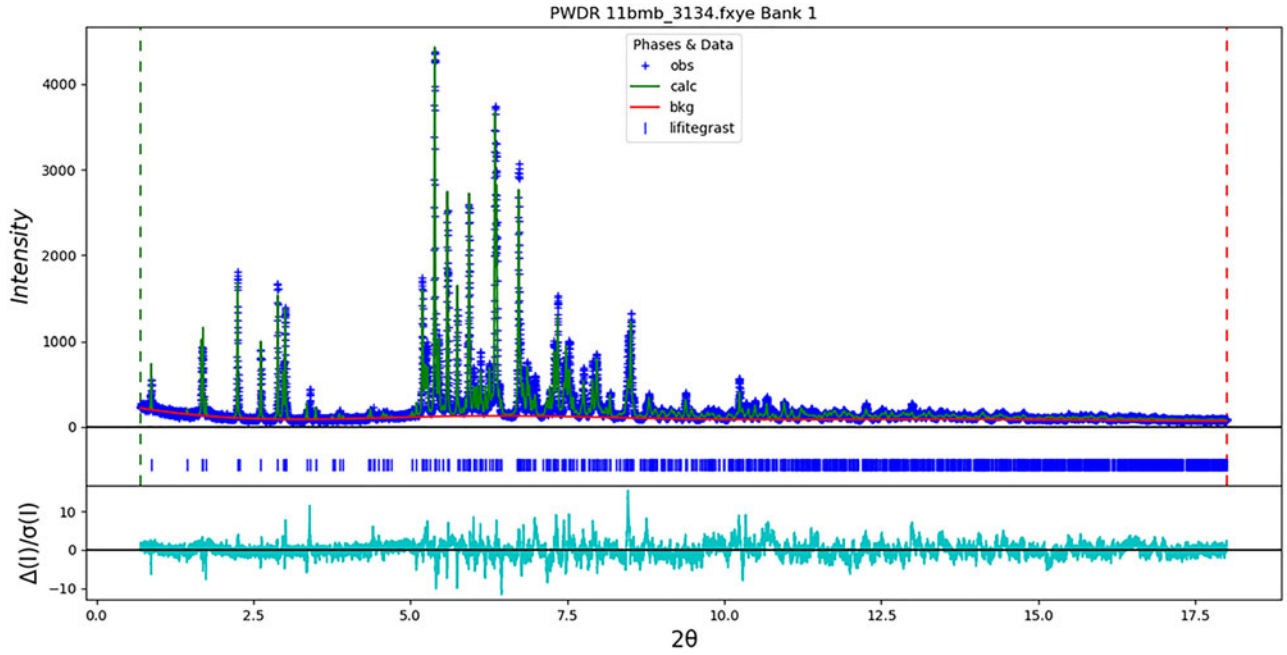

Figure 3. The Rietveld plot for the refinement of lifitegrast. The blue crosses represent the observed data points, and the green line is the calculated pattern. The cyan curve is the normalized error plot, and the red line is the background curve.

peaks, and probably indicate deficiency of the structural model.

The crystal structure of lifitegrast was optimized (fixed experimental unit cell) with density functional techniques using VASP (Kresse and Furthmüller, 1996) through the MedeA graphical interface (Materials Design, 2024). The calculation was carried out on 32 cores of a 144-core (768 GB memory) HPE Superdome Flex 280 Linux server at North Central College. The calculation used the GGA-PBE functional, a plane wave cutoff energy of 400.0 eV, and a *k*-point spacing of 0.5 $Å^{-1}$ leading to a $1 \times 3 \times 1$ mesh, and took ~48 h. Single-point density functional calculations (fixed experimental cell) and population analysis were carried out using CRYSTAL23 (Erba et al., 2023). The basis sets for the H, C, N and O atoms in the calculation were those of Gatti et al. (1994), and those for Cl and S were those of Peintinger et al. (2013). The calculations were run on a 3.5 GHz PC using 8 *k*-points and the B3LYP functional, and took ~9 h.

III. RESULTS AND DISCUSSION

The powder pattern of this study is similar enough to that reported by Burnier et al. (2013) to suggest that they probably represent the same material (Figure 2). The patent states: "A mass loss of about 2.5% between room temperature and 18.0°C is observed. From the coupled FTIR analysis carried out simultaneously, the loss is attributable to loss of water. Without being bound by theory, the results suggest that Form A is a hydrate, with a theoretical mass loss of 2.8%". A monohydrate corresponds to weight loss of 2.8%. The previously mentioned three water sites found in this study refine with occupancies very close to unity, suggesting that our material is a sesquihydrate, which would correspond to a mass loss due to water loss of 4.2%. Perhaps the water content in Form A is variable.

The root-mean-square (rms) Cartesian displacement of the non-H atoms in the Rietveld-refined and VASP-optimized molecules is 0.631 Å for molecule 1 (the lower atom numbers) (Figure 4) and 0.549 Å for molecule 2 (Figure 5). The agreement is outside the normal range for correct structures (van de Streek and Neumann, 2014). The absolute positions of the lifitegrast molecules are similar (Figure 6), showing that the structure reported here is at least a good local minimum (if not the global minimum). This is a large structure refined with a limited data set, so perhaps we should expect less accuracy than usual. The displacement coefficients of some atoms refined to very large values (Figure 7), and are highlighted in Figure 8. As illustrated in Figure 9, the two independent lifitegrast molecules have very different conformations (rms Cartesian displacement = 1.654 Å). The largest differences occur in regions with large displacement coefficients, so perhaps the large U_{iso} indicate disorder in the crystal. Since an ordered model is needed for the density functional theory (DFT) calculations, we have chosen to refine an ordered model, rather than to model any disorder. The structural model proposed here is just that – a proposed model. If someone else can derive a better model, we would be pleased. The remaining discussion will emphasize the VASP-optimized structure.

All of the bond distances, and most of the bond angles and torsion angles fall within the normal ranges indicated by a Mercury/Mogul Geometry check (Macrae et al., 2020). Five bond angles are flagged as unusual: C28–C24–C21 (127.3°; average = 120.1(23)°; *Z*-score = 3.2), C29–C24–C21 (112.2°; average = 120.3(25)°; *Z*-score = 3.1), C106–S68–C98 (108.9°; average = 104.5(11)°; *Z*-score = 4.0), C78–C80 = C83 (127.8°; average = 121.5(20)°; *Z*-score = 3.1), and C89–C86–N76 (125.6°; average = 118.7(13)°; *Z*-score = 5.3). The two largest *Z*-scores have exceptionally low uncertainties on the averages, inflating the *Z*-scores. Torsion angles involving rotations about the C21–N11, C32–C23, C90–C85, and C97–C88 bonds are flagged as unusual. They lie on the tails of broad

https://doi.org/10.1017/S0885715624000459 Published online by Cambridge University Press

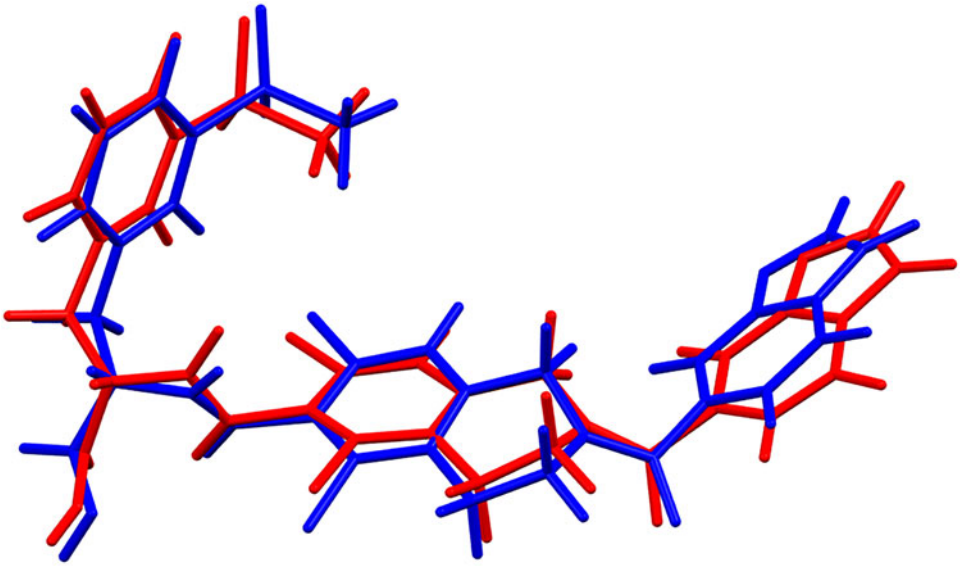

Figure 4. Comparison of the Rietveld-refined (red) and VASP-optimized (blue) structures of lifitegrast molecule 1. The rms Cartesian displacement is 0.631 Å. Image generated using Mercury (Macrae et al., 2020).

distributions and reflect the orientation of the carbonyl group and saturated ring in molecule 1, the orientation of the dichlorophenyl ring in molecule 2, and the orientations of both carboxylic acid groups. Some parts of both molecules seem to be slightly unusual, presumably reflecting solid-state effects on conformations.

Quantum chemical geometry optimization of the isolated molecules (DFT/B3LYP/6-31G*/water) using Spartan '24 (Wavefunction, 2023) indicated that molecule 2 is 2.0 kcal mol^{-1} higher in energy than molecule 1. The global minimum-energy conformation (MMFF) is much more compact, showing that intermolecular interactions are important to determining the solid-state conformations.

The crystal structure (Figure 6) consists of discrete lifitegrast molecules linked by hydrogen bonds among carboxylic acid groups, carbonyl groups, and water molecules into a three-dimensional framework. The water molecules occur in clusters. The volume/non-hydrogen atom is smaller than normal, at 16.7 $Å^3$.

Analysis of the contributions to the total crystal energy of the structure using the Forcite module of Materials Studio (Dassault Systèmes, 2023) indicates that angle distortion terms are most significant for the intramolecular distortion energy, but that torsion and bond terms also contribute. The intermolecular energy is dominated by electrostatic attractions, which in this force field analysis include hydrogen bonds. The hydrogen bonds are better analyzed using the results of the DFT calculation.

Both classical and non-classical hydrogen bonds (Table I) contribute to the lattice energy. Each water molecule acts as a

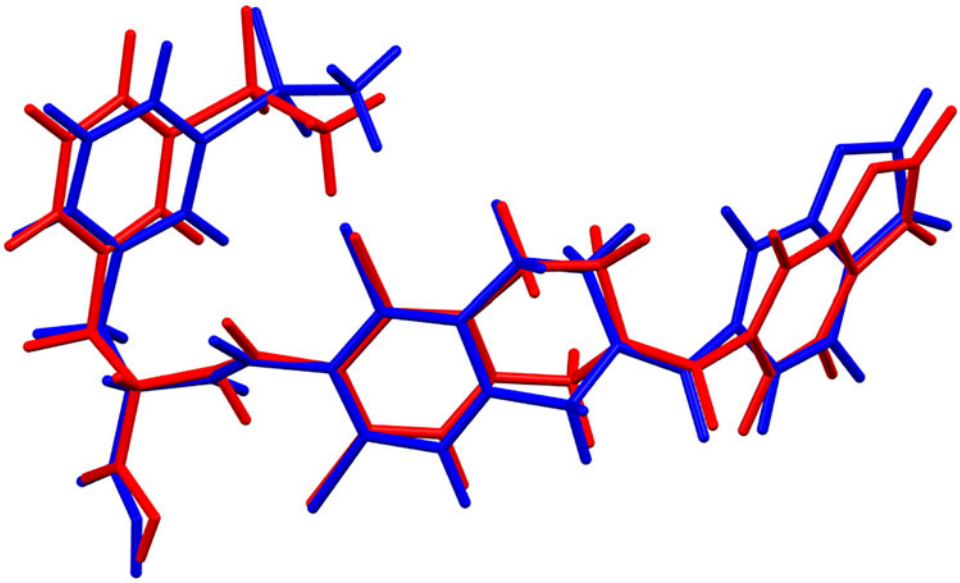

Figure 5. Comparison of the Rietveld-refined (red) and VASP-optimized (blue) structures of lifitegrast molecule 2. The rms Cartesian displacement is 0.549 Å. Image generated using Mercury (Macrae et al., 2020).

https://doi.org/10.1017/S0885715624000459 Published online by Cambridge University Press

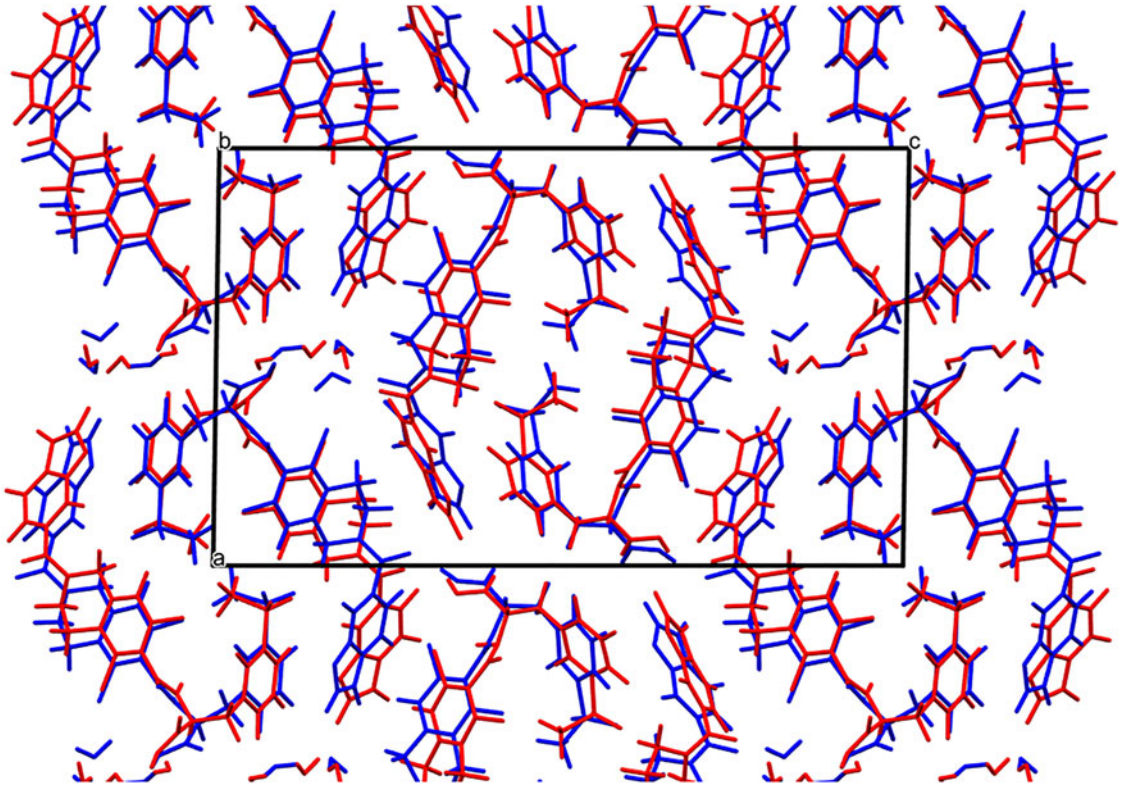

Figure 6. Comparison of the Rietveld-refined (red) and VASP-optimized (blue) crystal structures of lifitegrast Form A sesquihydrate. The view is down the *b*-axis, and the image was generated using Mercury (Macrae et al., 2020).

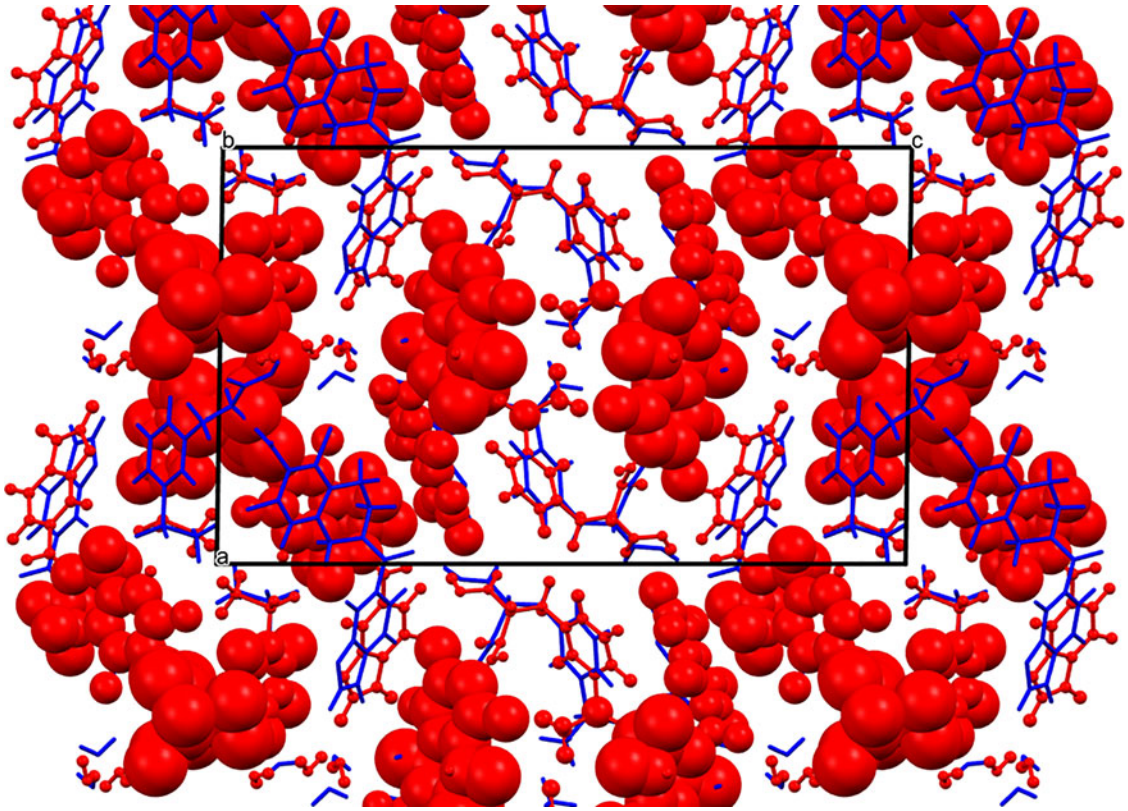

Figure 7. Comparison of the Rietveld-refined (red) and VASP-optimized (blue) crystal structures of lifitegrast Form A sesquihydrate, with the atoms in the experimental structure pictures as 50% displacement spheroids. The view is down the *b*-axis, and the image was generated using Mercury (Macrae et al., 2020).

https://doi.org/10.1017/S0885715624000459 Published online by Cambridge University Press

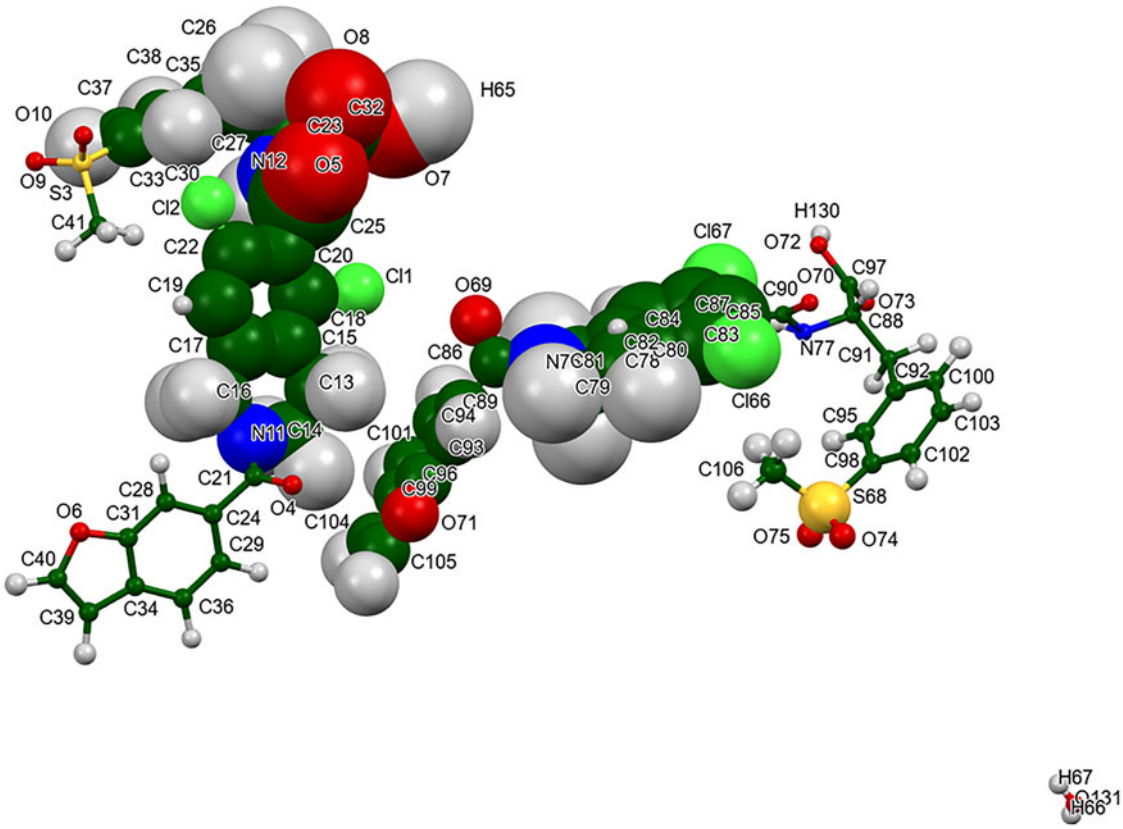

Figure 8. The asymmetric unit of lifitegrast Form A sesquihydrate, with the atom numbering. The atoms are represented by 50% probability spheroids. Image generated using Mercury (Macrae et al., 2020).

donor in two O–H···O hydrogen bonds, and as an acceptor. Water molecule O137 acts as an acceptor in a water–water O–H···O hydrogen bond, and all three water molecules are acceptors in C–H···O hydrogen bonds. Each carboxylic acid group acts as a donor in a strong discrete O–H···O hydrogen bond; molecule 1 to a water molecule and molecule 2 to a carbonyl group. The energies of the O–H···O hydrogen bonds were calculated using the correlation of Rammohan and Kaduk (2018). The amino groups N12 and N77 both form N–H···O hydrogen bonds to carbonyl groups. The energies of the N–H···O hydrogen bonds were calculated using the correlation of Wheatley and Kaduk (2019). Many C–H···O

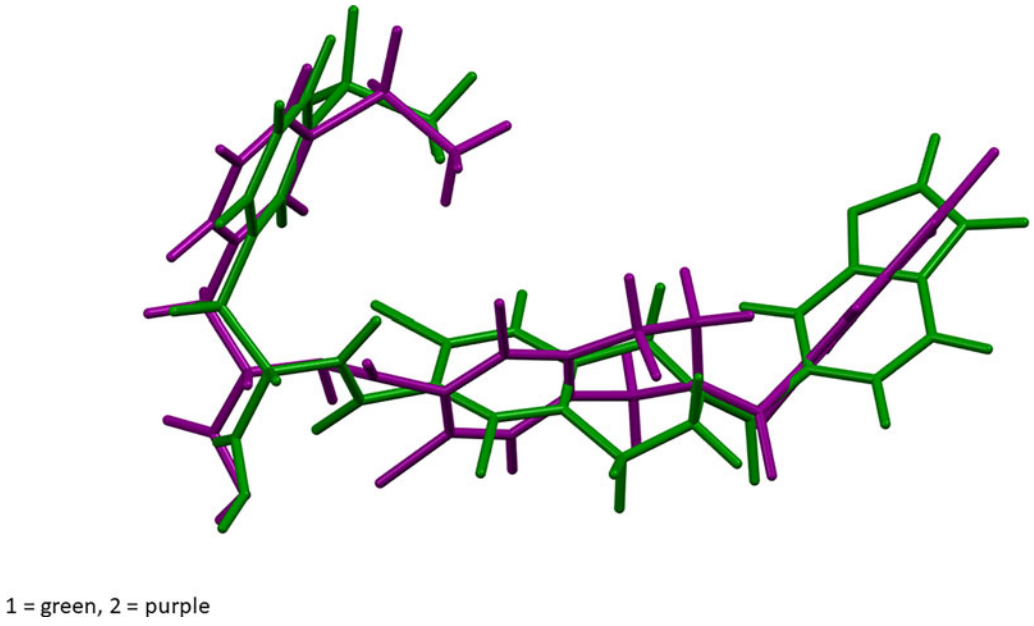

Figure 9. Comparison of molecule 1 (green) and molecule 2 (purple) in the structure of lifitegrast Form A sesquihydrate. The rms displacement is 1.654 Å. Image generated using Mercury (Macrae et al., 2020).

https://doi.org/10.1017/S0885715624000459 Published online by Cambridge University Press

TABLE I. Hydrogen bonds (CRYSTAL23) in lifitegrast.

H-Bond	D–H (Å)	H···A (Å)	D···A (Å)	D–H···A (°)	Overlap (*e*)	E (kcal mol^{-1})
O137–H71···O132	1.004	1.647	2.647	173.2	0.067	14.1
O137–H70···O69	0.986	1.844	2.828	174.9	0.043	11.3
O132–H69···O7	0.974	2.192	2.808	119.9	0.018	7.3
O132–H68···O69	0.988	1.716	2.651	156.5	0.046	11.7
O131–H67···O7	0.977	2.328	3.228	152.8	0.020	7.7
O131–H66···O137	1.015	1.620	2.629	172.5	0.081	15.5
C94–H57···O132	1.089	2.686	3.650	147.4	0.015	
C40–H54···O137	1.086	2.430	3.412	149.8	0.017	
C26–H51···O131	1.097	2.366	3.340	147.0	0.023	
O72–H130···O4	1.011	1.721	2.708	164.4	0.065	13.9
O7–H65···O131	1.058	1.491	2.548	176.0	0.089	16.3
N77–H117···O70	1.028	1.957	2.919	154.5	0.045	4.9
N12–H52···O5	1.024	2.247	3.248	165.1	0.030	4.0
C105–H74···O73	1.088	2.296	3.343	161.0	0.031	
C104–H73···O4	1.086	2.934	3.990	164.0	0.011	
C106–H128···O75	1.096	2.034	3.086	160.0	0.039	
C88–H114···O70	1.103	2.403[a]	2.864	103.2	0.010	
C81–H111···O69	1.092	2.162[a]	2.574	99.3	0.010	
C79–H109···O74	1.096	2.696	3.369	119.2	0.010	
C37–H41···O6	1.087	2.329	3.151	131.0	0.012	
C35–H39···O7	1.090	2.667	3.753	174.1	0.014	
C28–H36···O9	1.89	2.833	3.839	153.6	0.010	
C19–H35···O10	1.089	2.603	3.525	141.9	0.012	
C41–H61···O10	1.096	2.195	3.174	147.4	0.026	
C23–H49···O8	1.102	2.222	3.214	148.5	0.019	
C14–H45···O4	1.093	2.299[a]	2.770	103.7	0.015	
C78–H108···Cl66	1.095	2.758[a]	3.166	101.8	0.011	
C41–H62···Cl2	1.097	2.592	3.650	161.8	0.019	
C13–H43···Cl1	1.100	2.707[a]	3.029	96.1	0.010	
C84–H55···C39	1.091	2.633	3.713	170.1	0.013	

[a]Intramolecular.

and C–H···Cl hydrogen bonds also contribute to the lattice energy.

The Bravais–Friedel–Donnay–Harker (Bravais, 1866; Friedel, 1907; Donnay and Harker, 1937) morphology suggests that we might expect needle morphology for lifitegrast, with <010> as the long axis (as expected from the anisotropy of the lattice parameters). A fourth-order spherical harmonic model was included in the refinement. The texture index was 1.064(2), indicating that preferred orientation was small in this rotated capillary specimen.

IV. DEPOSITED DATA

The powder pattern of lifitegrast sesquihydrate Form A from this synchrotron data set has been submitted to ICDD for inclusion in the Powder Diffraction File. The Crystallographic Information Framework (CIF) files containing the results of the Rietveld refinement (including the raw data) and the DFT geometry optimization were deposited with the ICDD. The data can be requested at pdj@icdd.com.

ACKNOWLEDGEMENTS

The use of the Advanced Photon Source at Argonne National Laboratory was supported by the U.S. Department of Energy, Office of Science, Office of Basic Energy Sciences, under Contract No. DE-AC02-06CH11357. This work was partially supported by the International Centre for Diffraction Data. We thank Saul Lapidus for his assistance in the data collection.

CONFLICTS OF INTEREST

The authors have no conflicts of interest to declare.

REFERENCES

Altomare, A., C. Cuocci, C. Giacovazzo, A. Moliterni, R. Rizzi, N. Corriero, and A. Falcicchio. 2013. "EXPO2013: A Kit of Tools for Phasing Crystal Structures from Powder Data." *Journal of Applied Crystallography* 46: 1231–35.

Antao, S. M., I. Hassan, J. Wang, P. L. Lee, and B. H. Toby. 2008. "State-of-the-Art High-Resolution Powder X-Ray Diffraction (HRPXRD) Illustrated with Rietveld Refinement of Quartz, Sodalite, Tremolite, and Meionite." *Canadian Mineralogist* 46: 1501–09.

Blanton, J., R. Papoular, and D. Louër. 2019. "PreDICT: A Graphical User Interface to the DICVOL14 Indexing Software Program for Powder Diffraction Data." *Powder Diffraction* 34: 233–41.

Bravais, A. 1866. *Etudes Cristallographiques*. Gauthier Villars.

Bruno, I. J., J. C. Cole, M. Kessler, J. Luo, W. D. S. Motherwell, L. H. Purkis, B. R. Smith, R. Taylor, R. I. Cooper, S. E. Harris, and A. G. Orpen. 2004. "Retrieval of Crystallographically-Derived Molecular Geometry Information." *Journal of Chemical Information and Computer Sciences* 44: 2133–44.

Burnier, J., T. Gadek, and F. Naud. 2013. "Crystalline Pharmaceutical and Methods of Preparation and Use Thereof." United States Patent 8.367,701 B2.

Dassault Systèmes. 2023. *BIOVIA Materials Studio 2024*. BIOVIA.

Donnay, J. D. H., and D. Harker. 1937. "A New Law of Crystal Morphology Extending the Law of Bravais." *American Mineralogist* 22: 446–67.

https://doi.org/10.1017/S0885715624000459 Published online by Cambridge University Press

Erba, A., J. K. Desmarais, S. Casassa, B. Civalleri, L. Donà, I. J. Bush, B. Searle, L. Maschio, L.-E. Daga, A. Cossard, C. Ribaldone, E. Ascrizzi, N. L. Marana, J.-P. Flament, and B. Kirtman. 2023. "CRYSTAL23: A Program for Computational Solid State Physics and Chemistry." *Journal of Chemical Theory and Computation* 19: 6891–932. doi:10.1021/acs.jctc.2c00958.

Friedel, G. 1907. "Etudes sur la loi de Bravais." *Bulletin de la Société Française de Minéralogie* 30: 326–455.

Gatti, C., V. R. Saunders, and C. Roetti. 1994. "Crystal-Field Effects on the Topological Properties of the Electron-Density in Molecular Crystals – The Case of Urea." *Journal of Chemical Physics* 101: 10686–96.

Groom, C. R., I. J. Bruno, M. P. Lightfoot, and S. C. Ward. 2016. "The Cambridge Structural Database." *Acta Crystallographica Section B: Structural Science, Crystal Engineering and Materials* 72: 171–79.

Kabekkodu, S., A. Dosen, and T. N. Blanton. 2024. "PDF-5+: A Comprehensive Powder Diffraction File™ for Materials Characterization." *Powder Diffraction* 39: 47–59.

Kaduk, J. A., C. E. Crowder, K. Zhong, T. G. Fawcett, and M. R. Suchomel. 2014. "Crystal Structure of Atomoxetine Hydrochloride (Strattera), $C_{17}H_{22}NOCl$." *Powder Diffraction* 29: 269–73.

Kim, S., J. Chen, T. Cheng, A. Gindulyte, J. He, S. He, Q. Li, B. A. Shoemaker, P. A. Thiessen, B. Yu, L. Zaslavsky, J. Zhang, and E. E. Bolton. 2023. "PubChem 2023 Update." *Nucleic Acids Research* 51 (D1): D1373–80. doi:10.1093/nar/gkac956.

Kresse, G., and J. Furthmüller. 1996. "Efficiency of Ab-Initio Total Energy Calculations for Metals and Semiconductors Using a Plane-Wave Basis Set." *Computational Materials Science* 6: 15–50.

Lee, P. L., D. Shu, M. Ramanathan, C. Preissner, J. Wang, M. A. Beno, R. B. Von Dreele, L. Ribaud, C. Kurtz, S. M. Antao, X. Jiao, and B. H. Toby. 2008. "A Twelve-Analyzer Detector System for High-Resolution Powder Diffraction." *Journal of Synchrotron Radiation* 15: 427–32.

Louër, D., and A. Boultif. 2014. "Some Further Considerations in Powder Diffraction Pattern Indexing with the Dichotomy Method." *Powder Diffraction* 29: S7–12.

Macrae, C. F., I. Sovago, S. J. Cottrell, P. T. A. Galek, P. McCabe, E. Pidcock, M. Platings, G. P. Shields, J. S. Stevens, M. Towler, and P. A. Wood. 2020. "*Mercury 4.0*: From Visualization to Design and Prediction." *Journal of Applied Crystallography* 53: 226–35.

Materials Design. 2024. *MedeA 3.7.2*. Materials Design Inc.

MDI. 2024. *JADE Pro Version 9.0*. Materials Data.

Peintinger, M. F., D. Vilela Oliveira, and T. Bredow. 2013. "Consistent Gaussian Basis Sets of Triple-Zeta Valence with Polarization Quality for Solid-State Calculations." *Journal of Computational Chemistry* 34: 451–59.

Rammohan, A., and J. A. Kaduk. 2018. "Crystal Structures of Alkali Metal (Group 1) Citrate Salts." *Acta Crystallographica Section B: Crystal Engineering and Materials* 74: 239–52. doi:10.1107/S2052520618002330.

Silk Scientific. 2013. *UN-SCAN-IT 7.0*. Silk Scientific Corporation.

Stephens, P. W. 1999. "Phenomenological Model of Anisotropic Peak Broadening in Powder Diffraction." *Journal of Applied Crystallography* 32: 281–89.

Sykes, R. A., P. McCabe, F. H. Allen, G. M. Battle, I. J. Bruno, and P. A. Wood. 2011. "New Software for Statistical Analysis of Cambridge Structural Database Data." *Journal of Applied Crystallography* 44: 882–86.

Toby, B. H., and R. B. Von Dreele. 2013. "GSAS II: The Genesis of a Modern Open Source All Purpose Crystallography Software Package." *Journal of Applied Crystallography* 46: 544–49.

van de Streek, J., and M. A. Neumann. 2014. "Validation of Molecular Crystal Structures from Powder Diffraction Data with Dispersion-Corrected Density Functional Theory (DFT-D)." *Acta Crystallographica Section B: Structural Science, Crystal Engineering and Materials* 70: 1020–32.

Wang, J., B. H. Toby, P. L. Lee, L. Ribaud, S. M. Antao, C. Kurtz, M. Ramanathan, R. B. Von Dreele, and M. A. Beno. 2008. "A Dedicated Powder Diffraction Beamline at the Advanced Photon Source: Commissioning and Early Operational Results." *Review of Scientific Instruments* 79: 085105.

Wavefunction, Inc. 2023. *Spartan '24. V. 1.0.0*. Wavefunction Inc.

Wheatley, A. M., and J. A. Kaduk. 2019. "Crystal Structures of Ammonium Citrates." *Powder Diffraction* 34: 35–43.